

Detailed and Reduced Dynamic Models of Passive and Active Limited-slip Car Differentials

Riccardo Morselli[†], Roberto Zanasi[†], Germano Sandoni[‡]
(December 6, 2004)

Passive and active limited slip differentials are used in high performance cars to optimize the torque distribution on the driving wheels for traction maximization, driving comfort, stability and active safety of the vehicle. In the paper, detailed and reduced dynamic models for the simulation of four kinds of differential are presented.

The models refer to the limited slip steering differential with two clutches. The model of the conventional differential, of the mechanical limited slip differential and of the controlled limited slip differential can be obtained by simplification. The detailed model allows the simulation of the internal phenomena that influence the differential dynamics. The reduced model focuses only on the main dynamic behavior of the differential. Some simulations show the use of the reduced model to compare the effects of the four differentials on the vehicle dynamics.

2000 Mathematics Subject Classification: 37M05, 91B74, 93A30.

Keywords: Limited-slip differential, dynamic models, simulation, variable dynamic dimension systems, vehicle handling.

1 Introduction

The differential (see Fig. 2) is a mechanism that allows the driving wheels to rotate at different speeds as they follow different paths around a corner, and yet both transmit torque to the ground. They are mounted on each car. The role of the differential has come under much scrutiny due to its strong influence on vehicle stability, control and traction, see [1].

The importance of the differential can be understood by studying the typical behaviour of the tires, Fig. 1 shows the basic principles, see [2] for further details. The dynamics of a wheel is given by:

$$J_w \dot{\omega} = \tau_w - F_x R_e$$

[†] D.I.I. University of Modena and Reggio Emilia, Via Vignolese 905/b, 41100, Modena, Italy.

[‡] Elektrics Elektronik Engineering, MAGNA STEYR Fahrzeugtechnik AG&Co KG, Liebenauer Hauptstrasse 317, A-8041 Graz, Austria.

where ω is the wheel angular velocity, J_w and R_e are the wheel inertia and rolling radius, τ_w is the driving torque and F_x is the longitudinal force generated by the tire contact patch. In a steady state condition the traction torque τ_w on a wheel corresponds to the tire longitudinal force $\tau_w \simeq F_x R_e$ (neglecting the rolling resistance) and the tires exhibit a small slip λ defined as:

$$\lambda = \frac{R_e \omega - v_x}{v_x}$$

where v_x is the longitudinal wheel speed. When the torque on the wheels exceeds the corresponding maximum longitudinal force F_{xm} that the tire can transmit to the ground (i.e. $\tau_w > F_{xm} R_e$), the tire starts spinning, the slip λ tends to increase, and both the longitudinal F_x and the lateral F_y forces transmitted to the ground sharply decrease, see Fig. 1. While cornering, the decrease of the lateral force F_y due to the wheel spinning can be very dangerous for the stability of the vehicle because a further slight increment of the car speed leads to a strong vehicle oversteer (rear wheel drive) or understeer (front wheel drive). Moreover, the decrease of a tire longitudinal force F_x due to the spinning reduces the car acceleration.

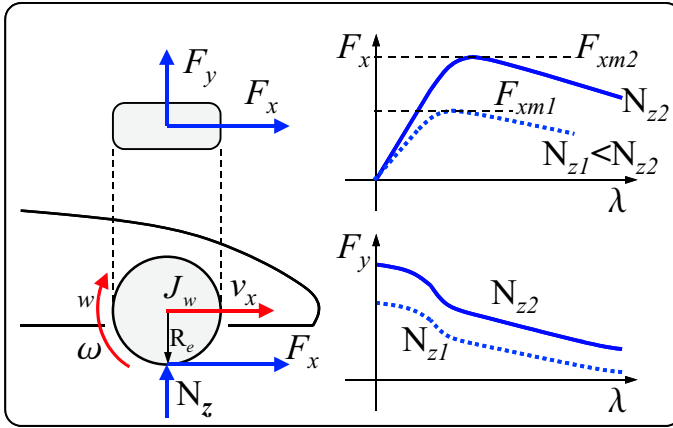


Figure 1. Basic tire behaviour: slip and vertical load effects on longitudinal and lateral forces.

To avoid the wheel spinning during cornering, the Vehicle Dynamic Control (VDC) and the Electronic Stability Program (ESP) systems, see [3] and [4], operate on the wheel brake pressures and on the engine in order to reduce the generated torque. This solution is good for safety, but it is not optimal in terms of performances: brakes dissipate energy and the reduction of the engine torque limits the longitudinal acceleration. Proper differentials are used to overcome these drawbacks.

The maximum longitudinal force F_{xm} that a tire can transmit to the ground is limited. During cornering, the lateral acceleration causes a load transfer from the inner wheel to the outer wheel. Since the maximum longitudinal force F_{xm} of a tire increases as the vertical load N_z increases (see Fig. 1), the outer wheel can transmit more torque to the ground with respect to the inner one. This is the basic principle to understand the differential control strategies. Note that different torques on the driving wheels introduce a steering effect on the car, therefore the controlled differentials can be seen as yaw control systems.

The conventional open differential delivers equal torque to each wheel, independently of the relative speed of the two wheels. During cornering, since the inner wheel has a lower vertical load, it starts spinning before the outer wheel. When it happens, the car starts understeering, the engine torque must be reduced to stop the wheel spinning and therefore the longitudinal acceleration is limited.

The mechanical limited-slip differential uses one or two clutches to establish a Coulomb friction between the two differential output shafts (the two half shafts). This friction is proportional to the total torque delivered to the differential case and it depends on the sign of the wheels relative speed; it subtracts torque from the fastest wheel and adds the same torque to the slowest wheel. In normal conditions the inner wheel is slower than the outer one, therefore any acceleration produces an unpleasant understeer effect (i.e. more torque is delivered to the inner wheel) with respect to the car equipped with the conventional differential. The benefits of a mechanical limited-slip differential are clear when the inner wheel starts spinning: its speed is greater than the speed of the outer wheel and therefore torque is transferred from the inner to the outer wheel. This automatically reduces the wheel spinning, and more torque is transmitted to the wheel that has the higher vertical load improving the acceleration performances of the car.

For the mechanical limited-slip differential, the amplitude of the friction depends on the input torque from the propeller shaft. The electronically controlled limited-slip differential (briefly electronic differential) is similar to the mechanical one, but uses an electro-actuated wet clutch and therefore more control flexibility is gained. Essentially, the electronic differential is activated (i.e. friction is added) only when the inner wheel tends to spin. By this way, the benefits of the mechanical limited-slip differential at high lateral acceleration are kept, at the same time the unpleasant understeer effect at low lateral acceleration disappears.

A further evolution is the electronically controlled “steering” differential sketched in Fig. 2. This mechanical solution overcome the common problem of the other differentials: it can transfer torque from the inner to the outer wheel even if the outer wheel is faster than the inner. The electronic steering differential has important effects on the vehicle stability thanks to its ability to

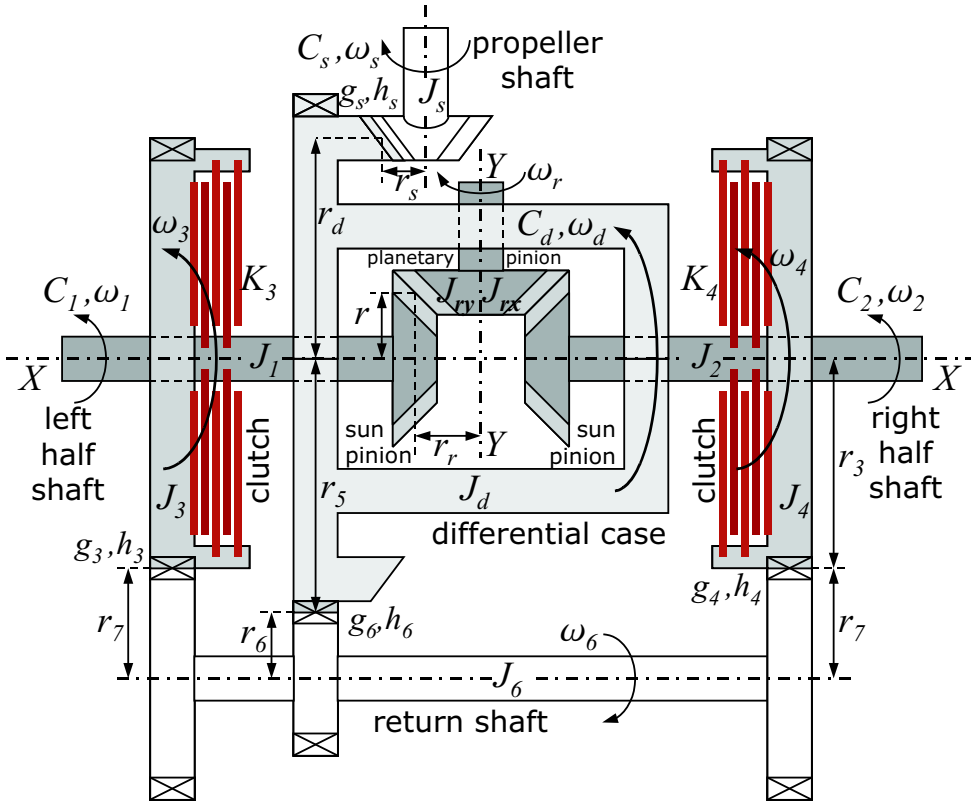


Figure 2. Mechanical scheme of the steering differential.

steer the car by controlling the torque difference between the two half shafts.

The limited-slip differentials have strong effects on vehicle safety, stability and performances. The development of proper control strategies requires differential and vehicle models for the simulation of the vehicle dynamics and for the control algorithms testing. Moreover, the ESP control system must interact with the electronic differentials to achieve the best performances. The development of an integrated control strategy is under investigation and differential mathematical models for simulation are essential. This paper proposes three models of the electronically controlled *steering differential* with different levels of detail for the simulation of the differential behaviour and for the simulation of vehicle dynamics. Moreover, these models can be easily used to simulate the dynamic behaviour of all the other kinds of differentials.

The paper is organized as follows: the mechanical description and the detailed mathematical model of the steering differential are introduced in Sec. 2. The complex detailed mathematical model is then reduced and simplified in Sec. 3. The reduced model is used in Sec. 4 to compare in simulation the be-

haviours of the four kinds of differentials. Finally some conclusions are drawn.

2 Steering Differential with Control Clutches

A simplified mechanical scheme of a steering differential is shown in Fig. 2. The propeller shaft J_s transmits the torque C_s from the engine (through the gearbox) to the differential case J_d . The differential case rotates around the $X - X$ axis and drags the *planet pinions* J_r (for simplicity only one planet pinion is shown in Fig. 2). The planet pinions are connected to the two half shafts J_1 and J_2 by means of the two *sun pinions*. Let's define the following gear ratios:

$$D_c = \frac{r_d}{r_s}, \quad D_r = \frac{r_r}{r}, \quad D_t = \frac{r_7}{r_3}, \quad D_k = \frac{r_6}{r_5}$$

When ideal gears are considered (no lash and infinite stiffness), the following ratios between angular velocities hold:

$$D_c = \frac{\omega_s}{\omega_d}, \quad D_r = \frac{\omega_1 - \omega_2}{\omega_r}, \quad D_t = \frac{\omega_3}{\omega_6} = \frac{\omega_4}{\omega_6}, \quad D_k = \frac{\omega_d}{\omega_6}$$

In a steady-state condition with ideal gears and no friction losses, the case angular velocity ω_d is the average of the two half shafts velocities ω_1 and ω_2 , and the torque $C_d = C_s D_c$ on the case is shared between the two shafts:

$$\omega_d = \frac{\omega_1 + \omega_2}{2} \quad C_1 = C_2 = \frac{C_d}{2} = \frac{C_s D_c}{2} \quad (1)$$

The structure described till now is the same as the conventional open differential. The electronically controlled steering differential adds the horizontal *return shaft* J_6 , the two *return wheels* J_3 and J_4 , and the two clutches K_3 (between J_3 and J_1) and K_4 (between J_4 and J_2). Due to the gear ratios, the following relations hold:

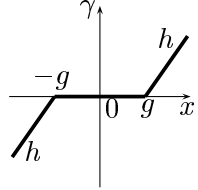
$$\omega_3 = \omega_4 = \frac{D_t}{D_k} \omega_d \quad \frac{D_t}{D_k} > 1$$

Let ω_2 represents the inner wheel velocity, in normal conditions it is $\omega_1 = \omega_d + \Delta\omega$, $\omega_2 = \omega_d - \Delta\omega$ with $\Delta\omega > 0$. If $\Delta\omega$ satisfies:

$$\Delta\omega < \omega_d \left(\frac{D_t}{D_k} - 1 \right) \quad \Rightarrow \quad \omega_3 > \omega_1$$

When the clutch K_3 is slipping and $\omega_3 > \omega_1$, the friction torque $K_3 \operatorname{sgn}(\omega_3 - \omega_1)$ delivers torque to the external wheel even if it is faster than the inner one, therefore the steering differential has a wider operating region than the other type of differentials.

To introduce the dynamic equations of a steering differential, let us define the function $\gamma(x, g, h)$ as follows:

$$\gamma(x, g, h) = \begin{cases} 0 & \text{if } |x| \leq g \\ h(x - g) & \text{if } x > g \\ h(x + g) & \text{if } x < -g \end{cases}$$


The function $\gamma(x, g, h)$ is used to describe both the torsional stiffness and the lash of a mechanical gearing. The parameter h represents the torsional stiffness and the parameter g describes the semi-amplitude of the lash. An ideal gearing with constant ratio has $g = 0$ and $h \rightarrow \infty$.

Let θ_i (for $i = 1, 2, 3, 4, 6$), θ_d , θ_r and θ_s denote the angular positions of the mechanical elements shown in Fig. 2. The proposed model of the car differential shown in Fig. 2 is described by the following dynamic equations:

$$\left\{ \begin{array}{l} \dot{\theta}_i = \omega_i \quad (\text{for } i = 1, 2, 3, 4, 6) \\ \dot{\theta}_d = \omega_d, \quad \dot{\theta}_r = \omega_r, \quad \dot{\theta}_s = \omega_s \\ J_s \dot{\omega}_s = C_s - b_s \omega_s - \gamma(\theta_s - D_c \theta_d, g_s, h_s) \\ J_1 \dot{\omega}_1 = C_1 - b_1 \omega_1 + K_3 \operatorname{sgn}(\omega_3 - \omega_1) + \gamma(\theta_d + D_r \theta_r - \theta_1, g_1, h_1) \\ J_2 \dot{\omega}_2 = C_2 - b_2 \omega_2 + K_4 \operatorname{sgn}(\omega_4 - \omega_2) + \gamma(\theta_d - D_r \theta_r - \theta_2, g_2, h_2) \\ J_{dx} \dot{\omega}_d = (J_d + J_{rx}) \dot{\omega}_d = -b_d \omega_d + \\ \quad + D_c \gamma(\theta_s - D_c \theta_d, g_s, h_s) - \gamma(\theta_d - D_k \theta_6, g_6, h_6) + \\ \quad - \gamma(\theta_d + D_r \theta_r - \theta_1, g_1, h_1) - \gamma(\theta_d - D_r \theta_r - \theta_2, g_2, h_2) \\ J_{ry} \dot{\omega}_r = D_r (\gamma(\theta_d - D_r \theta_r - \theta_2, g_2, h_2) - \gamma(\theta_d + D_r \theta_r - \theta_1, g_1, h_1)) - b_r \omega_r \\ J_3 \dot{\omega}_3 = +\gamma(D_t \theta_6 - \theta_3, g_3, h_3) - b_3 \omega_3 - K_3 \operatorname{sgn}(\omega_3 - \omega_1) \\ J_4 \dot{\omega}_4 = +\gamma(D_t \theta_6 - \theta_4, g_4, h_4) - b_4 \omega_4 - K_4 \operatorname{sgn}(\omega_4 - \omega_2) \\ J_6 \dot{\omega}_6 = D_k \gamma(\theta_d - D_k \theta_6, g_6, h_6) - b_6 \omega_6 + \\ \quad - D_t (\gamma(D_t \theta_6 - \theta_3, g_3, h_3) + \gamma(D_t \theta_6 - \theta_4, g_4, h_4)) \end{array} \right. \quad (2)$$

The linear friction $b_i \omega_i$ can be easily substituted by a generic nonlinear friction $b_i(\omega_i)$. The dynamic system defined by equations (2) can be simulated

by using the block scheme shown in Fig. 3. The basic idea of this scheme is to use the power interaction between subsystems as basic concept for modeling, see [5] and [6]. The dashed lines represent the power ports between the subsystems and the inner product of the two vectorial variables involved in each dashed line of the graph has the physical meaning of the power flowing through the section. The black dot means a change of sign. The presence of the integrators (integral causality) and the absence of derivators (differential causality), see [7], allow the reliable simulation of this scheme using every computer simulation. The matrices in the scheme of Fig. 3 are defined as follows:

$$\begin{aligned} \mathbf{J}_1 &= \text{diag}\{J_s, J_1, J_2\}, & \mathbf{J}_2 &= \text{diag}\{J_{dx}, J_{ry}, J_3, J_4\}, \\ \mathbf{B}_1 &= \text{diag}\{b_s, b_1, b_2\}, & \mathbf{B}_2 &= \text{diag}\{b_d, b_r, b_3, b_4\}, \end{aligned}$$

$$\mathbf{W}_1 = \begin{bmatrix} 1 & 0 & 0 & 0 & 0 \\ 0 & -1 & 0 & -1 & 0 \\ 0 & 0 & -1 & 0 & -1 \end{bmatrix}, \quad \mathbf{W}_2 = \begin{bmatrix} 1 & 0 & 0 \\ 0 & 0 & 0 \\ 0 & -1 & 0 \\ 0 & 0 & -1 \end{bmatrix},$$

$$\mathbf{D}_{cr} = \begin{bmatrix} D_c & -1 & -1 & 0 & 0 \\ 0 & -D_r & D_r & 0 & 0 \\ 0 & 0 & 0 & -1 & 0 \\ 0 & 0 & 0 & 0 & -1 \end{bmatrix}, \quad \mathbf{D}_{kt} = [D_k \quad -D_t \quad -D_t],$$

$$\begin{aligned} \mathbf{K}_s &= \text{diag}\{0, 0, 0, K_3 \text{sgn}(\cdot), K_4 \text{sgn}(\cdot)\}, \\ \mathbf{G}_1 &= \text{diag}\{\gamma(\cdot, g_s, h_s), \gamma(\cdot, g_1, h_1), \gamma(\cdot, g_2, h_2), 0, 0\}, \\ \mathbf{G}_2 &= \text{diag}\{\gamma(\cdot, g_6, h_6), \gamma(\cdot, g_3, h_3), \gamma(\cdot, g_4, h_4)\}. \end{aligned}$$

3 Model Reduction

The model of Fig. 3 corresponding to the system (2) requires a demanding computational effort to be simulated for two reasons. First the gears are usually almost ideal therefore the stiffness values h_s, h_1, h_2, h_3, h_4 and h_6 are very high. High stiffness values involve wide torque variations for small torsion angles, this slows down the simulations because the simulation step

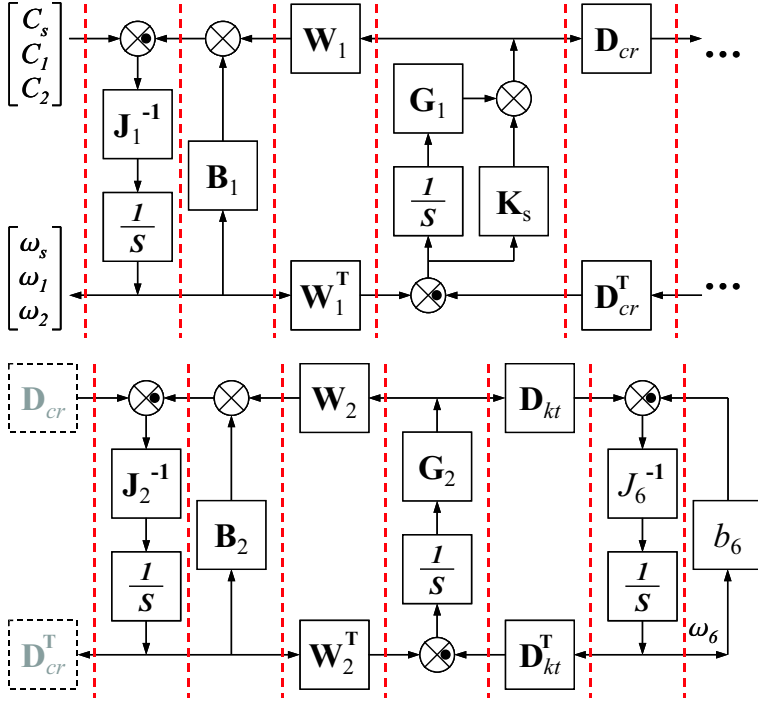


Figure 3. Scheme for the simulation of the steering differential corresponding to equations (2).

size must be reduced to achieve reliable results.

The second reason is the presence of the two terms $K_3 \operatorname{sgn}(\omega_3 - \omega_1)$ and $K_4 \operatorname{sgn}(\omega_4 - \omega_2)$ due to the Coulomb friction. When the difference $(\omega_i - \omega_j)$ becomes zero, the term $K_i \operatorname{sgn}(\omega_i - \omega_j)$ starts switching between $\pm K_i$, and to achieve reliable simulation results the simulation step size must be as small as possible. The problem of the proper simulation of Coulomb friction is a well studied subject and various solutions are present in literature. A survey of friction models and simulation techniques concerning the Coulomb friction is given in [8]. Some energy based accurate solutions can be found in [9]. The solution proposed in this paper differs from the preceding thanks to a state space transformation that allows to deal with the Coulomb friction without the need of models switching, pre-slip velocities, hybrid resistive ports. The simulation results are exact and the simulations only require the detection of the zero relative velocity. Moreover, the solutions presented in [8] and [9] are not applicable directly to the steering differential.

From a system theory point of view, the steering differential is a so called *Variable Dynamic Dimension System* (see [10]). Due to strong nonlinearities (i.e. $K_i \operatorname{sgn}(\omega_i - \omega_j)$), this kind of system changes its dynamic dimension during

normal system operations. The variable dynamic dimension systems are quite common in mechanical devices with Coulomb friction, such as clutches [11], gearboxes [12], brakes and limited slip differentials. From a mathematical point of view, the system order reduction means that some state variable derivatives are constrained to remain zero until some dynamical conditions are satisfied. In the steering differential, if the friction coefficient K_3 (or K_4) is high enough, the two inertia J_1 and J_3 (or J_2 and J_4) are constrained to rotate at the same speed: $\omega_1 = \omega_3$ (or $\omega_2 = \omega_4$) and the dynamic dimension is reduced by 1. When the dynamic dimension in the real system reduces, the term $K_3 \operatorname{sgn}(\omega_1 - \omega_3)$ (or $K_4 \operatorname{sgn}(\omega_2 - \omega_4)$) in model (2) starts switching and the computational effort rises dramatically. This problem can be solved using twice the algorithm presented in [10] for the two inertia pairs J_1, J_3 and J_2, J_4 . Nevertheless, the computational time remains affected by the high stiffness values.

This section presents step by step a model reduction that preserves the main dynamic behaviours of the steering differential and reduces significantly the simulation computational effort without affecting the reliability of the results.

First of all, since the gears are almost ideal, the lashes g_s, g_1, g_2, g_3, g_4 and g_6 are very small and their effect can be neglected. Reducing the lashes g_s, g_1, g_2, g_3, g_4 and g_6 to zero, the function $\gamma(x, g, h)$ simplifies as follows:

$$\gamma(x, 0, h) = h x$$

and the system (2) becomes:

$$\left\{ \begin{array}{l} J_s \dot{\omega}_s = C_s - b_s \omega_s - \xi_s \\ J_1 \dot{\omega}_1 = C_1 - b_1 \omega_1 + \xi_1 + K_3 \operatorname{sgn}(\omega_3 - \omega_1) \\ J_2 \dot{\omega}_2 = C_2 - b_2 \omega_2 + \xi_2 + K_4 \operatorname{sgn}(\omega_4 - \omega_2) \\ J_{dx} \dot{\omega}_d = D_c \xi_s - \xi_1 - \xi_2 - \xi_6 - b_d \omega_d \\ J_{ry} \dot{\omega}_r = D_r (\xi_2 - \xi_1) - b_r \omega_r \\ J_3 \dot{\omega}_3 = \xi_3 - b_3 \omega_3 - K_3 \operatorname{sgn}(\omega_3 - \omega_1) \\ J_4 \dot{\omega}_4 = \xi_4 - b_4 \omega_4 - K_4 \operatorname{sgn}(\omega_4 - \omega_2) \\ J_6 \dot{\omega}_6 = D_k \xi_6 - D_t (\xi_3 + \xi_4) - b_6 \omega_6 \\ \dot{\xi}_s = h_s (\omega_s - D_c \omega_d) \\ \dot{\xi}_1 = h_1 (\omega_d + D_r \omega_r - \omega_1) \\ \dot{\xi}_2 = h_2 (\omega_d - D_r \omega_r - \omega_2) \\ \dot{\xi}_3 = h_3 (D_t \omega_6 - \omega_3) \\ \dot{\xi}_4 = h_4 (D_t \omega_6 - \omega_4) \\ \dot{\xi}_6 = h_6 (\omega_d - D_k \omega_6) \end{array} \right. \quad (3)$$

The system (3) can be simulated by using the block scheme of Fig. 3 with the two matrices \mathbf{G}_1 and \mathbf{G}_2 changed as follows:

$$\mathbf{G}_1 = \text{diag}\{h_s, h_1, h_2, 0, 0\}, \quad \mathbf{G}_2 = \text{diag}\{h_6, h_3, h_4\}.$$

Let us rewrite system (3) in the following compact matrix form:

$$\begin{cases} \mathbf{L} \dot{\mathbf{x}} = \mathbf{A} \mathbf{x} - \mathbf{D}^T \mathbf{K}_s \text{sgn}(\mathbf{D} \mathbf{x}) + \mathbf{C}^T \mathbf{u} \\ \mathbf{y} = \mathbf{C} \mathbf{x} \end{cases} \quad (4)$$

where:

$$\mathbf{L} = \begin{bmatrix} J_s & 0 & 0 & 0 & 0 & 0 & 0 & 0 & 0 & 0 & 0 & 0 & 0 & 0 & 0 \\ 0 & J_1 & 0 & 0 & 0 & 0 & 0 & 0 & 0 & 0 & 0 & 0 & 0 & 0 & 0 \\ 0 & 0 & J_2 & 0 & 0 & 0 & 0 & 0 & 0 & 0 & 0 & 0 & 0 & 0 & 0 \\ 0 & 0 & 0 & \frac{1}{h_s} & 0 & 0 & 0 & 0 & 0 & 0 & 0 & 0 & 0 & 0 & 0 \\ 0 & 0 & 0 & 0 & \frac{1}{h_1} & 0 & 0 & 0 & 0 & 0 & 0 & 0 & 0 & 0 & 0 \\ 0 & 0 & 0 & 0 & 0 & \frac{1}{h_2} & 0 & 0 & 0 & 0 & 0 & 0 & 0 & 0 & 0 \\ 0 & 0 & 0 & 0 & 0 & 0 & J_{dx} & 0 & 0 & 0 & 0 & 0 & 0 & 0 & 0 \\ 0 & 0 & 0 & 0 & 0 & 0 & 0 & J_{ry} & 0 & 0 & 0 & 0 & 0 & 0 & 0 \\ 0 & 0 & 0 & 0 & 0 & 0 & 0 & 0 & \frac{1}{h_6} & 0 & 0 & 0 & 0 & 0 & 0 \\ 0 & 0 & 0 & 0 & 0 & 0 & 0 & 0 & 0 & J_6 & 0 & 0 & 0 & 0 & 0 \\ 0 & 0 & 0 & 0 & 0 & 0 & 0 & 0 & 0 & 0 & \frac{1}{h_3} & 0 & 0 & 0 & 0 \\ 0 & 0 & 0 & 0 & 0 & 0 & 0 & 0 & 0 & 0 & 0 & \frac{1}{h_4} & 0 & 0 & 0 \\ 0 & 0 & 0 & 0 & 0 & 0 & 0 & 0 & 0 & 0 & 0 & 0 & 0 & J_3 & 0 \\ 0 & 0 & 0 & 0 & 0 & 0 & 0 & 0 & 0 & 0 & 0 & 0 & 0 & 0 & J_4 \end{bmatrix}, \quad \mathbf{x} = \begin{bmatrix} \omega_s \\ \omega_1 \\ \omega_2 \\ \xi_s \\ \xi_1 \\ \xi_2 \\ \omega_d \\ \omega_r \\ \xi_6 \\ \omega_6 \\ \xi_3 \\ \xi_4 \\ \omega_3 \\ \omega_4 \end{bmatrix}, \quad \mathbf{D}^T = \begin{bmatrix} 0 & 0 \\ -1 & 0 \\ 0 & -1 \\ 0 & 0 \\ 0 & 0 \\ 0 & 0 \\ 0 & 0 \\ 0 & 0 \\ 0 & 0 \\ 0 & 0 \\ 0 & 0 \\ 0 & 0 \\ 1 & 0 \\ 0 & 1 \end{bmatrix},$$

$$\mathbf{K}_s = \begin{bmatrix} K_3 & 0 \\ 0 & K_4 \end{bmatrix}, \quad \mathbf{u} = \begin{bmatrix} C_s \\ C_1 \\ C_2 \end{bmatrix}, \quad \mathbf{y} = \begin{bmatrix} \omega_s \\ \omega_1 \\ \omega_2 \end{bmatrix},$$

$$\mathbf{A} = \begin{bmatrix} -b_s & 0 & 0 & -1 & 0 & 0 & 0 & 0 & 0 & 0 & 0 & 0 & 0 & 0 \\ 0 & -b_1 & 0 & 0 & 1 & 0 & 0 & 0 & 0 & 0 & 0 & 0 & 0 & 0 \\ 0 & 0 & -b_2 & 0 & 0 & 1 & 0 & 0 & 0 & 0 & 0 & 0 & 0 & 0 \\ 1 & 0 & 0 & 0 & 0 & 0 & -D_c & 0 & 0 & 0 & 0 & 0 & 0 & 0 \\ 0 & -1 & 0 & 0 & 0 & 0 & 1 & D_r & 0 & 0 & 0 & 0 & 0 & 0 \\ 0 & 0 & -1 & 0 & 0 & 0 & 1 & -D_r & 0 & 0 & 0 & 0 & 0 & 0 \\ 0 & 0 & 0 & D_c & -1 & -1 & -b_d & 0 & -1 & 0 & 0 & 0 & 0 & 0 \\ 0 & 0 & 0 & 0 & -D_r D_r & 0 & -b_r & 0 & 0 & 0 & 0 & 0 & 0 & 0 \\ 0 & 0 & 0 & 0 & 0 & 0 & 1 & 0 & 0 & -D_k & 0 & 0 & 0 & 0 \\ 0 & 0 & 0 & 0 & 0 & 0 & 0 & 0 & D_k & -b_6 & -D_t & -D_t & 0 & 0 \\ 0 & 0 & 0 & 0 & 0 & 0 & 0 & 0 & 0 & D_t & 0 & 0 & -1 & 0 \\ 0 & 0 & 0 & 0 & 0 & 0 & 0 & 0 & 0 & D_t & 0 & 0 & 0 & -1 \\ 0 & 0 & 0 & 0 & 0 & 0 & 0 & 0 & 0 & 0 & 1 & 0 & -b_3 & 0 \\ 0 & 0 & 0 & 0 & 0 & 0 & 0 & 0 & 0 & 0 & 0 & 1 & 0 & -b_4 \end{bmatrix}, \quad \mathbf{C}^T = \begin{bmatrix} 1 & 0 & 0 \\ 0 & 1 & 0 \\ 0 & 0 & 1 \\ 0 & 0 & 0 \\ 0 & 0 & 0 \\ 0 & 0 & 0 \\ 0 & 0 & 0 \\ 0 & 0 & 0 \\ 0 & 0 & 0 \\ 0 & 0 & 0 \\ 0 & 0 & 0 \\ 0 & 0 & 0 \\ 0 & 0 & 0 \\ 0 & 0 & 0 \\ 0 & 0 & 0 \end{bmatrix}.$$

Assuming ideal gears, the stiffness values h_1, h_2, h_3, h_4, h_6 and h_s tend to infinity, the last 6 equations of system (3) lead to 6 algebraic constraints:

$$\begin{cases} \omega_s = D_c \omega_d \\ \omega_1 = \omega_d + D_r \omega_r \\ \omega_2 = \omega_d - D_r \omega_r \\ \omega_d = D_k \omega_6 \\ \omega_3 = D_t \omega_6 \\ \omega_4 = D_t \omega_6 \end{cases} \implies \begin{cases} \omega_s = D_c \omega_d \\ \omega_d = \frac{\omega_1 + \omega_2}{2} \\ \omega_r = \frac{1}{D_r} \frac{\omega_1 - \omega_2}{2} \\ \omega_6 = \frac{\omega_d}{D_k} \\ \omega_3 = \frac{D_t}{D_k} \omega_d \\ \omega_4 = \omega_3 \end{cases} \quad (5)$$

Considering the algebraic equations (5) it is possible to find a rectangular state space transformation $\mathbf{x} = \mathbf{T} \mathbf{z}$ that reduces system (4) from the 14th to the second order:

$$\begin{array}{c}
\left[\begin{array}{c} \omega_s \\ \omega_1 \\ \omega_2 \\ \xi_s \\ \xi_1 \\ \xi_2 \\ \omega_d \\ \omega_r \\ \xi_6 \\ \omega_6 \\ \xi_3 \\ \xi_4 \\ \omega_3 \\ \omega_4 \end{array} \right] \\
\underbrace{\hspace{1.5cm}}_{\mathbf{x}}
\end{array}
=
\underbrace{\left[\begin{array}{cc}
D_c D_k D_r (D_k - D_t) & -D_c D_k D_r (D_k - D_t) \\
D_r (2D_k^2 - 3D_t D_k + D_t^2) & D_t D_r (D_t - D_k) \\
D_t D_r (D_k - D_t) & -D_r (2D_k^2 - 3D_t D_k + D_t^2) \\
0 & 0 \\
0 & 0 \\
0 & 0 \\
D_k D_r (D_k - D_t) & -D_k D_r (D_k - D_t) \\
(D_k - D_t)^2 & (D_k - D_t)^2 \\
0 & 0 \\
D_r (D_k - D_t) & D_r (D_t - D_k) \\
0 & 0 \\
0 & 0 \\
D_t D_r (D_k - D_t) & -D_t D_r (D_k - D_t) \\
D_t D_r (D_k - D_t) & -D_t D_r (D_k - D_t)
\end{array} \right]}_{\mathbf{T}}
\underbrace{\left[\begin{array}{c} z_1 \\ z_2 \end{array} \right]}_{\mathbf{z}} \quad (6)$$

Applying the congruent state space transformation (6) to system (4), one obtains the following simplified system:

$$\begin{cases} \mathbf{L}_T \dot{\mathbf{z}} = \mathbf{A}_T \mathbf{z} - \mathbf{D}_T^T \mathbf{K}_s \operatorname{sgn}(\mathbf{D}_T \mathbf{z}) + \mathbf{C}_T^T \mathbf{u} \\ \mathbf{y} = \mathbf{C}_T \mathbf{z} \end{cases} \quad (7)$$

where

$$\begin{aligned}
\mathbf{L}_T &= \mathbf{T}^T \mathbf{L} \mathbf{T} = \begin{bmatrix} l_{11} & l_{12} \\ l_{12} & l_{22} \end{bmatrix}, & \mathbf{A}_T &= \mathbf{T}^T \mathbf{A} \mathbf{T} = \begin{bmatrix} a_{11} & a_{12} \\ a_{12} & a_{22} \end{bmatrix}, \\
\mathbf{D}_T &= \mathbf{D} \mathbf{T} = \begin{bmatrix} -2D_r (D_k - D_t)^2 & 0 \\ 0 & 2D_r (D_k - D_t)^2 \end{bmatrix}, & & (8) \\
\mathbf{C}_T &= \mathbf{C} \mathbf{T} = \begin{bmatrix} D_c D_k D_r (D_k - D_t) & -D_c D_k D_r (D_k - D_t) \\ D_r (2D_k^2 - 3D_k D_t + D_t^2) & -D_r D_t (D_k - D_t) \\ D_r D_t (D_k - D_t) & -D_r (2D_k^2 - 3D_k D_t + D_t^2) \end{bmatrix}
\end{aligned}$$

Parameters l_{ij} and a_{ij} can be easily computed from the previously defined matrices \mathbf{L} , \mathbf{A} and \mathbf{T} . The matrices \mathbf{L}_T and \mathbf{A}_T are symmetric and nonsingular ($D_t \neq D_k$) and matrix \mathbf{D}_T is diagonal. The transformed system (7) is graphically described by the block scheme of Fig. 4.

The system (7) is simpler than system (4) because ideal gears have been considered, but the computational effort still remains demanding due to the presence of the two terms $K_i \operatorname{sgn}(\omega_i - \omega_j)$. The state space transformation \mathbf{T}

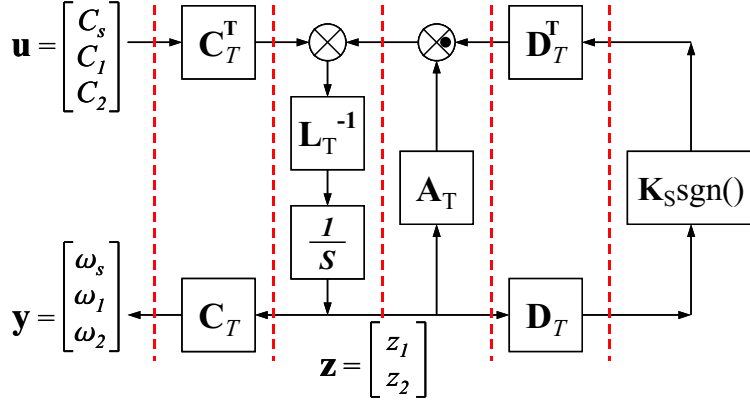


Figure 4. Scheme for the simulation of the reduced transformed system (7)

gives to system (7) an important property that allows to solve this problem. Since both \mathbf{D}_T and \mathbf{K}_s are diagonal, the vector $\mathbf{D}_T^T \mathbf{K}_s \text{sgn}(\mathbf{D}_T \mathbf{z})$ in system (7) simplifies as follows:

$$\mathbf{D}_T^T \mathbf{K}_s \text{sgn}(\mathbf{D}_T \mathbf{z}) = \begin{bmatrix} \overbrace{2D_r(D_k - D_t)^2 K_3 \text{sgn}(D_k - D_t)^2 \text{sgn}(z_1)}^{k_1} \\ \overbrace{2D_r(D_k - D_t)^2 K_4 \text{sgn}(D_k - D_t)^2 \text{sgn}(z_2)}^{k_2} \end{bmatrix} = \begin{bmatrix} k_1 \text{sgn}(z_1) \\ k_2 \text{sgn}(z_2) \end{bmatrix} \quad (9)$$

Namely the transformation \mathbf{T} has split the dynamic effect of the two terms $K_i \text{sgn}(\omega_i - \omega_j)$ on two different state variables. Let us denote:

$$\begin{bmatrix} F_1 \\ F_2 \end{bmatrix} = \mathbf{A}_T \mathbf{z} + \mathbf{C}_T^T \mathbf{u} \quad (10)$$

Using (9) and (10), system (7) can be rewritten in the following explicit form:

$$\begin{bmatrix} \dot{z}_1 \\ \dot{z}_2 \end{bmatrix} = \underbrace{\begin{bmatrix} J_{11} & J_{12} \\ J_{12} & J_{22} \end{bmatrix}}_{\mathbf{L}_T^{-1}} \begin{bmatrix} F_1 - k_1 \text{sgn}(z_1) \\ F_2 - k_2 \text{sgn}(z_2) \end{bmatrix} \quad (11)$$

Regarding system (11), when the variable z_i ($i = 1, 2$) is zero and when some dynamical conditions are satisfied, the function $k_i \text{sgn}(z_i)$ causes a sliding mode condition (see [13]) and the term $k_i \text{sgn}(z_i)$ starts switching at infinite frequency between the two values $\pm k_i$. This condition cannot be precisely simulated by computer. To cope with this problem, a proper simulation algorithm

has been designed to achieve fast and precise simulations.

Let τ_i denote the equivalent control associated to the switching term $k_i \operatorname{sgn}(z_i)$, that is the time mean value of the term $k_i \operatorname{sgn}(z_i)$. The equivalent control can be seen as the average value of the sliding variable and the system dynamics does not change if the sliding term $k_i \operatorname{sgn}(z_i)$ is substituted by the corresponding equivalent control τ_i .

When a sliding condition arises on the variable z_i , the function $k_i \operatorname{sgn}(z_i)$ holds $z_i = 0$, therefore the corresponding equivalent control τ_i can be computed by solving (11) with $\dot{z}_i = 0$. The sliding mode condition is maintained if the equivalent control τ_i satisfies the condition $|\tau_i| \leq k_i$. The simulation algorithm presented in [10] can be easily adapted to system (11). For this system, only 4 different cases are possible:

- 1) Let $z_1 \neq 0$ and $z_2 \neq 0$. Since the state variables are not zero, sliding mode conditions cannot arise and the system dynamics is given (and simulated) by (11).
- 2) Let $z_1 \neq 0$ and $z_2 = 0$. A sliding mode can arise on variable z_2 . The corresponding equivalent control τ_2 is the control necessary to hold the condition $z_2 = 0$, therefore it can be computed substituting $k_2 \operatorname{sgn}(z_2)$ with τ_2 in (11) and imposing the condition $\dot{z}_2 = 0$. The equation to be solved with respect to the equivalent control τ_2 is the following:

$$[0] = [J_{12} J_{22}] \begin{bmatrix} F_1 - k_1 \operatorname{sgn}(z_1) \\ F_2 - \tau_2 \end{bmatrix}$$

The equivalent control τ_2 necessary to hold the condition $z_2 = 0$ is then:

$$\tau_2 = F_2 + \frac{J_{12}}{J_{22}}(F_1 - k_1 \operatorname{sgn}(z_1)) \quad (12)$$

Since the condition $|\tau_2| \leq k_2$ must be satisfied, the dynamics of system (11) when $z_1 \neq 0$ and $z_2 = 0$ is given (and simulated) by:

$$\begin{bmatrix} \dot{z}_1 \\ \dot{z}_2 \end{bmatrix} = \begin{cases} \mathbf{L}_T^{-1} \begin{bmatrix} F_1 - k_1 \operatorname{sgn}(z_1) \\ F_2 - \tau_2 \end{bmatrix} & \text{if } |\tau_2| \leq k_2 \\ \mathbf{L}_T^{-1} \begin{bmatrix} F_1 - k_1 \operatorname{sgn}(z_1) \\ F_2 - k_2 \operatorname{sgn}(\tau_2) \end{bmatrix} & \text{if } |\tau_2| > k_2 \end{cases} \quad (13)$$

Until $|\tau_2| \leq k_2$ the equivalent control is able to hold $\dot{z}_2 = 0$ and consequently $z_2 = 0$. As soon as $|\tau_2| > k_2$ the derivative $\dot{z}_2 \neq 0$, then it follows $z_2 \neq 0$. The term $k_2 \operatorname{sgn}(\tau_2)$ means that the equivalent control τ_2 is

constrained between the values $\pm k_2$.

- 3) Let $z_1 = 0$ and $z_2 \neq 0$. The solution is symmetric with respect to case 2).
- 4) Let $z_1 = 0$ and $z_2 = 0$. The solution is similar to case 2). A sliding mode can arise on either z_1 or z_2 or both. The two corresponding equivalent controls τ_1 and τ_2 are computed solving the system:

$$\begin{bmatrix} 0 \\ 0 \end{bmatrix} = \mathbf{L}_T^{-1} \begin{bmatrix} F_1 - \tau_1 \\ F_2 - \tau_2 \end{bmatrix} \Rightarrow \begin{cases} \tau_1 = F_1 \\ \tau_2 = F_2 \end{cases} \quad (14)$$

Since the two conditions $|\tau_i| \leq k_i$ must be satisfied, the dynamics of system (11) when $z_1 = 0$ and $z_2 = 0$ is given (and simulated) by:

$$\begin{bmatrix} \dot{z}_1 \\ \dot{z}_2 \end{bmatrix} = \begin{cases} \mathbf{L}_T^{-1} \begin{bmatrix} F_1 - \tau_1 \\ F_2 - \tau_2 \end{bmatrix} = \begin{bmatrix} 0 \\ 0 \end{bmatrix} & \text{if } |\tau_1| \leq k_1 \text{ and } |\tau_2| \leq k_2 \\ \mathbf{L}_T^{-1} \begin{bmatrix} F_1 - \tau_1 \\ F_2 - k_2 \operatorname{sgn}(\tau_2) \end{bmatrix} & \text{if } |\tau_1| \leq k_1 \text{ and } |\tau_2| > k_2 \\ \mathbf{L}_T^{-1} \begin{bmatrix} F_1 - k_1 \operatorname{sgn}(\tau_1) \\ F_2 - \tau_2 \end{bmatrix} & \text{if } |\tau_1| > k_1 \text{ and } |\tau_2| \leq k_2 \\ \mathbf{L}_T^{-1} \begin{bmatrix} F_1 - k_1 \operatorname{sgn}(\tau_1) \\ F_2 - k_2 \operatorname{sgn}(\tau_2) \end{bmatrix} & \text{if } |\tau_1| > k_1 \text{ and } |\tau_2| > k_2 \end{cases} \quad (15)$$

This case seems to be the most complex, but it is the less interesting from the simulations point of view because the condition $z_1 = z_2 = 0$ means that the differential does not rotate and the car is at rest.

Please note that the simplicity of the proposed algorithm is due to the proper congruent transformation \mathbf{T} . The steering differential model is the most complex among the other kinds of differential. Mathematically this means that the dynamic behaviour of all the car differentials (see [14]) can be simulated by the steering differential model of Fig. 4. In fact, the inertias J_d , J_3 , J_4 and J_6 can be merged to represent the case inertia of a conventional, mechanical limited-slip or electronic limited-slip differential. Moreover, thanks to the wider operating region of the steering differential, the torque imbalance between the two half shafts of the other differentials can be easily obtained with proper values of the two friction coefficients K_3 and K_4 .

4 Simulation Results and Comparisons

The simulations described in this section refer to a car cornering a 10 m constant radius left curve at constant longitudinal acceleration $a_x = 0.3g$. In the sequel the behaviours of the four kinds of differential are compared using the model (7). Fig. 5 shows the vertical loads and the lateral acceleration of the car along the corner. The tires are described by Pacejka formula [2] with parameters corresponding to a commercial tire, see Fig. 6.

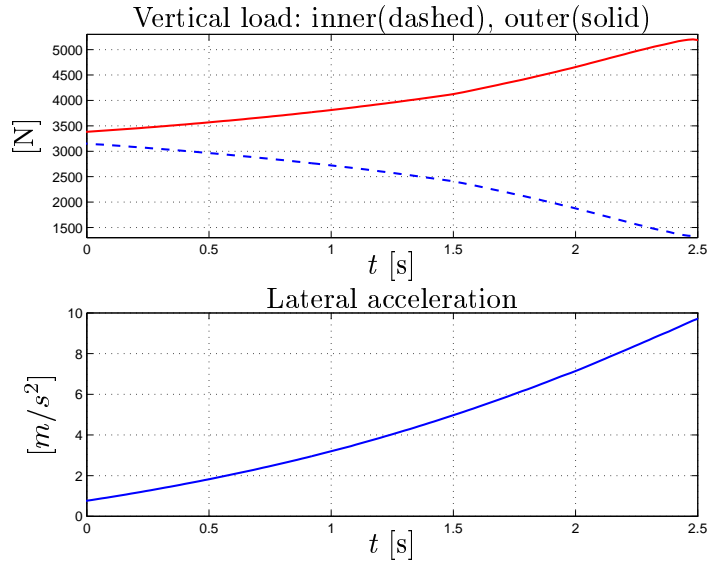


Figure 5. Vertical load and lateral acceleration for a 10m radius curve at longitudinal acceleration $a_x = 0.3g$.

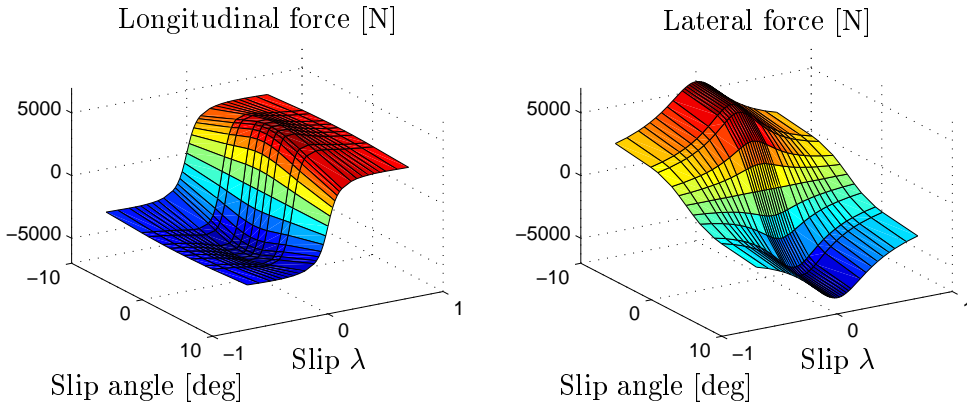


Figure 6. Tire characteristics at constant vertical load (4900N) by Pacejka formula.

The torques delivered to the two half shafts and the wheel speeds when the conventional differential is used are shown in Fig. 7. For $t < 1.8$ s the speed and the lateral acceleration are low, both driving wheels well adhere to the road surface and the outer wheel rotates at a higher speed than the inner one. This is the normal driving condition. For $t > 1.8$ s the vertical load on the inner wheel becomes low enough to cause the inner wheel spinning. This spinning is due to the fact that the torque on the two half shafts is the same.

The mechanical limited-slip differential avoids the inner wheel spinning because for $t > 1.8$ s more torque is delivered to the outer wheel, see Fig. 8. The two wheel speeds are equal because the differential is locked due to the total torque delivered to the differential case. The drawback is that for low lateral acceleration the car has a tendency for understeering (with respect to the car equipped with the conventional differential) because the inner wheel gets more torque.

The understeer drawback is solved with the electronic limited-slip differential as shown in Fig. 9. The differential is locked only for $t > 1.8$ s, as soon as the inner wheel speed becomes greater than the outer one. For low lateral acceleration the behaviour is the same as the conventional differential.

Finally, Fig. 10 underlines the capability of the electronically controlled steering differential to deliver the desired torque on the two wheels when condition (1) is satisfied. In the simulation of Fig. 10, the torque difference between the two wheels follows the lateral load transfer.

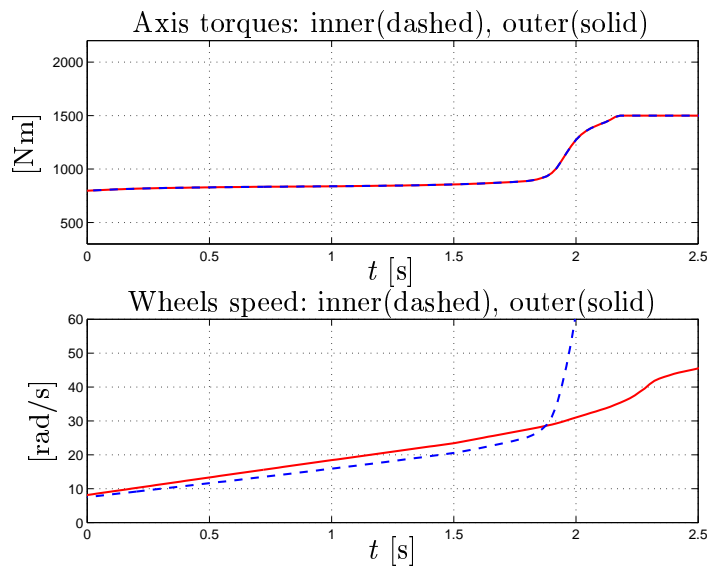


Figure 7. Axis torques and wheels speed with the conventional differential.

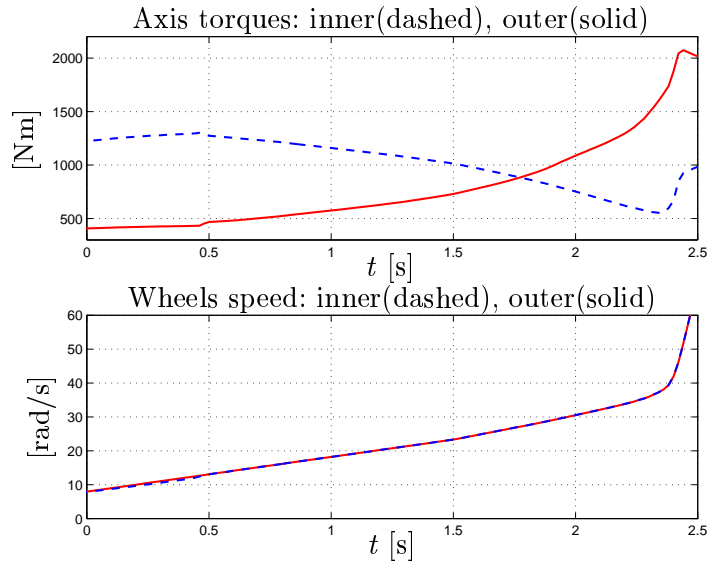


Figure 8. Axis torques and wheels speed with the mechanical limited-slip differential.

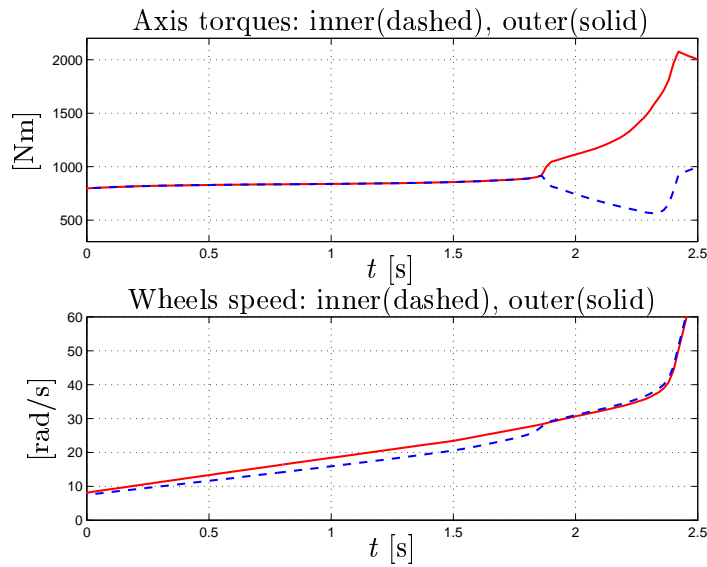


Figure 9. Axis torques and wheels speed with the electronic limited-slip differential.

5 Conclusions

A detailed dynamic model of an electronically controlled steering differential has been proposed. To obtain faster and still reliable simulations, reduced dynamic models have been obtained by a proper state-space transformation and

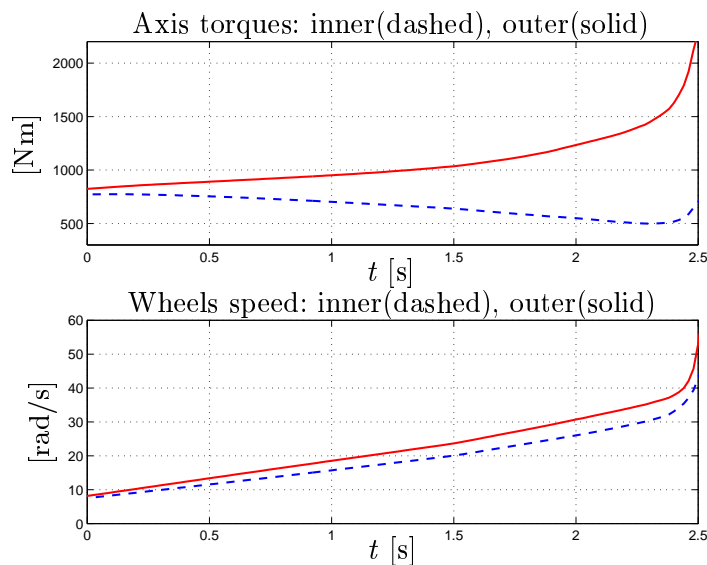


Figure 10. Axis torques and wheels speed with the electronic steering differential.

simplification of the detailed model. The steering differential models allow the simulation of the dynamical behaviour of the most common car differentials. The proposed reduced model has been used to compare the effects of four kinds of differentials on the vehicle dynamics.

References

- [1] P. Wright, "Formula 1 Technology", SAE book, ISBN 0-7680-0234-6, 2000, pp 82-91.
- [2] H.B. Pacejka, "Tyre and Vehicle Dynamics". SAE book, ISBN 0-7680-1126-4, 2002.
- [3] A.T. van Zanten, R. Erhardt, G. Pfaff, "VDC, The Vehicle Dynamics Control System of Bosch", SAE Technical Paper Series, no. 950759, 1995.
- [4] A.T. van Zanten, "Bosch ESP Systems: 5 Years of Experience", SAE Technical Paper Series, no. 2000-01-1633, 2000.
- [5] D. C. Karnopp, R. C. Rosenberg, "System dynamics: a unified approach", Wiley, N.Y, 1975.
- [6] R. Zanasi, "Power Oriented Modelling of Dynamical System for Simulation", IMACS Symp. on Modelling and Control of Technological System, Lille, France, May 1991.
- [7] P.C. Breedveld, "Port-Based Modeling of Mechatronic Systems", in: Mathematics and Computer in Simulations, n.66, pp. 99-127, 2004.
- [8] B. Armstrong-Hlouvrya, P. Dupont and C. Canudas De Wit: "A Survey of Models, Analysis Tools and Compensation Methods for the Control of Machines with Friction", Automatica. v.30, n.7, July 1994, Pages 1083-1138.
- [9] P.C. Breedveld, "An alternative Model for Static and Dynamic Friction in Dynamic System Simulation", preprints 1st IFAC conference on Mechatronic Systems, 2000, Darmstadt, Germany, pp. 717-722, 2000.
- [10] R. Zanasi, G. Sandoni, R. Morselli, "Simulation of a Variable Dynamic Dimension Systems: the clutch example", European Control Conference (ECC), Porto (Portugal), Settembre 2001.
- [11] R. Zanasi, A. Visconti, G. Sandoni, R. Morselli, "Dynamic Modeling and Control of a Car Transmission System", International Conference on Advanced Intelligent Mechatronics, Como, Italy, 2001.
- [12] R. Zanasi, G. Sandoni, A. Visconti, "Dynamic Model and Control of a Gearbox System", Mechatronics Forum International Conference, Enschede (Netherlands), June 2002.

- [13] V.I. Utkin, "Variable Structure Systems with Sliding Modes", IEEE Trans. Automatic Control, Vol. 22, pp. 212-222, (1977).
- [14] R. Zanasi, G. Sandoni, R. Morselli: "Mechanical and Active Car Differential: Detailed and Reduced Dynamic Models", proceedings of the Symposium on Mathematical Modelling - MATH-MOD'03, Vien, Austria, pp. 1011-1020, ISBN:3-901608-24-9, February 2003.